ABC 11 - Program – DAY 1
Lecture theatre 505-011, Grafton Campus

3rd Dec 2018	
8.00am	Registration open
8.30am to 9.00am	Opening Ceremony
9.00 am to 10.30 am Session Chairs: A/Prof Sam Veres and Dr Geoff Hansfield	**CLINICAL BIOMECHANICS I** **Invited Speaker** – **Prof Peter Hunter** University of Auckland - ABI On: MAPPING THE AUTONOMIC NERVOUS SYSTEM **Scientific Presentations** • Hip muscle activation in femoroacetabular impingement syndrome – Laura Diamond (Griffith University) • Validation of automated clinical gait assessment using a smart knee brace – Andrew McDaid (University of Auckland) • How pelvic tilt influences modes of spinal motion segment failure under direct compression - Nurul Haiza (Zaza) Sapiee (University of Auckland) • The effects of heel lifts on lower limb biomechanics – Chantel Rabusin (La Trobe University) • Combined EMG-informed neuromusculoskeletal and surrogates of finite element models estimate localised Achilles tendon strain in real-time – Claudio Pizzolato (Griffith University)

HIP MUSCLE ACTIVATION IN FEMOROACETABULAR IMPINGEMENT SYNDROME

[1,2]Laura Diamond, [2]Wolbert Van den Hoorn, [3]Kim Bennell, [3]Tim Wrigley, [3]Rana Hinman, [4]John O'Donnell, [2]Paul Hodges

[1]Griffith University, Menzies Health Institute Queensland, School of Allied Health Sciences, QLD, Australia
[2]The University of Queensland, Centre of Clinical Research Excellence in Spinal Pain, QLD, Australia
[3]The University of Melbourne, Centre for Health, Exercise and Sports Medicine, VIC, Australia
[4]St Vincent's Hospital, East Melbourne, VIC, Australia

INTRODUCTION

Deep hip muscle retraining is a common objective of non-operative management and post-operative rehabilitation for femoroacetabular impingement (FAI) syndrome [1]. These muscles are considered to have an important role in hip joint stabilization and may contribute to intra-articular loading and tissue health. It is unclear whether their function is altered in the presence of hip pathology. An understanding of deep hip muscle function in FAI syndrome is needed to inform targeted treatment programs. This exploratory study aimed to investigate activation patterns of the deep and superficial hip muscles during two squatting tasks: (i) an unconstrained deep squat where participants could use their preferred strategy to reach maximum depth; and (ii) a constrained squat designed to encourage deep hip flexion without allowing for compensation from the trunk or pelvis, in individuals with FAI syndrome and an asymptomatic control group without FAI morphology. These tasks were designed to encourage motion towards a position of impingement, where control of the hip would be expected to be more challenging with potential to expose neuromuscular adaptations that may not be apparent in less challenging tasks.

METHOD

Fifteen individuals with FAI syndrome (symptoms, clinical examination and imaging (alpha angle >55° (cam FAI), and lateral centre edge angle >39° and/or positive crossover sign (combined FAI))) and 14 age- and sex-comparable controls without morphological FAI underwent testing. Intramuscular fine-wire and surface electrodes recorded electromyographic (EMG) activity of selected deep and superficial hip muscles during the tasks. EMG data from both squatting tasks were amplitude-normalized to the mean of the peak values during the ascending phase of the unconstrained squat. Activation patterns were compared between groups for both types of squats using a wavelet-based linear mixed effects model based on the technique of wavelet functional ANOVA [2] ($p < 0.05$). A contraction ratio was calculated to compare activation levels during the descent and ascent phases of the tasks. Participant contraction ratios, averaged across squatting trials, were compared between-groups for each task using independent t-tests ($p < 0.05$).

RESULTS

The FAI and control groups were comparable for age, sex and body mass index. There were no between-group differences for squat depth or speed during descent or ascent for either task. Participants with FAI exhibited patterns of activation that differed significantly to controls across all muscles when squatting using their preferred strategy. For both tasks, participants with FAI exhibited a pattern of activation for obturator internus during descent that was similar in amplitude to ascent (Figure 1), despite the contrasting contraction modes (i.e. eccentric vs concentric).
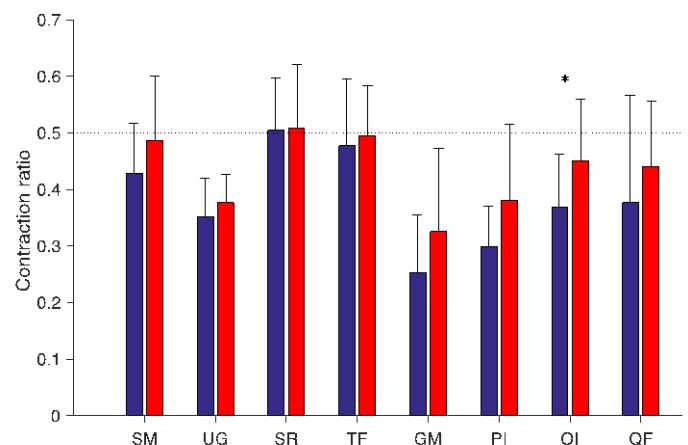

Figure 1. Ensemble average (+standard deviation) contraction ratios for control (blue) and FAI participants during the unconstrained squat. A ratio of 0.5 indicates equal contraction during descent and ascent phases. SM - semimembranosus; UG - gluteus maximus; SR - sartorius; TF - tensor fasciae latae; GM - gluteus medius; PI - piriformis; OI - obturator internus; QF - quadratus femoris; *p<0.05

CONCLUSIONS

Deep and superficial hip muscle activation is altered during squatting in individuals with FAI syndrome. Individuals with FAI syndrome do not differentiate between descent and ascent, and appear to implement a protective strategy as the hip descends towards impingement. Future studies should examine patients prospectively to establish whether these strategies are counterproductive for pathology and warrant rehabilitation.

REFERENCES

1. Bennell, KL et al. BMC MuscDisord 15:58, 2014.
2. McKay J et al. *Neurophysiol* 109: 591-602, 2013.

SPEAKER INFORMATION

Laura Diamond – l.diamond@griffith.edu.au

VALIDATION OF AUTOMATED CLINICAL GAIT ASSESSMENT USING A SMART KNEE BRACE

A Alder[1], A Davis[1] and A McDaid[1, 2]
[1]University of Auckland, [2]OPUM Technologies Ltd

INTRODUCTION

Gait analysis has many clinical and research applications, for example monitoring the recovery of people who have had knee injuries or surgeries. Many methods exist for gait analysis e.g. video gait assessment, gait mat systems (e.g. GAITRite®), or marker and marker-less optical motion capture. This abstract presents the use of a smart knee brace as an alternative means of gait analysis which can be easily used in the field by an untrained user. Figure 1 below illustrates the Digital Knee™, a wearable system used for this study which has in-built proprietary algorithms for stride detection and spatiotemporal gait parameters.

Figure 1. Digital Knee™.

METHOD

We validated the smart knee brace with two common clinical gait assessments; (1) a 10m gait test and (2) a six-minute gait test. Three trials of each assessment were conducted by five healthy participants (Table 1).

Table 1. Participant Details.

	Participant Number				
	1	2	3	4	5
Sex	M	M	F	M	M
Age	24	23	22	21	22
Height (m)	1.73	1.76	1.57	1.90	1.92
Weight (kg)	73	75	62	80	98

The 10m walk test was conducted in a 10m straight walking track, and a 7m diameter circle was used for the 6 minute walk test. The algorithm outputs produced by the Digital Knee™ were compared with the assessor's manual measurements to determine the difference.

RESULTS

The average percentage error for the two gait assessments are displayed in Table 1 and Table 2. Notably, only two of the five participants had any stride detection error across both gait tests (10 out of

345 and 5 out of 285 strides were missed for participants 3 and 4, respectively). Overall, the average stride detection error was 0.94%. The gait time parameter had a maximum error of 1.3% in the 10m walk test and 0.31% in the 6 minute walk test. The error related to distance was higher with maximum of 12.50% and 9.85% and averages of 6.87% and 5.42% in the 10 m and 6 minute walk tests, respectively.

Table 1. 10m walk test.

Participant Number	Average Percentage Error				
	Stride Detection	Total Distance	Total Time	Average Stride Length	Average Stride Time
1	0.00	0.82	0.39	0.75	0.30
2	0.00	0.94	0.33	0.91	0.20
3	0.00	12.50	1.30	12.50	1.01
4	0.00	11.37	0.65	11.18	0.96
5	0.00	8.70	0.11	8.70	0.34
Average	0.00	6.87	0.55	6.81	0.56

Table 2. 6 minute walk test.

Participant Number	Average Percentage Error				
	Stride Detection	Total Distance	Total Time	Average Stride Length	Average Stride Time
1	0.00	4.03	0.16	3.99	0.17
2	0.00	2.36	0.11	2.15	0.43
3	2.90	-	-	-	-
4	1.78	-	-	-	-
5	0.00	9.85	0.31	9.71	0.24
Average	0.94	5.42	0.19	5.29	0.28

Gait parameter errors for participants 3 and 4 for the 6 minute walk test were omitted given the errors are related to the missed strides.

CONCLUSIONS

In this pilot trial the spatiotemporal gait parameter algorithms in the Digital Knee™ smart knee brace were found to perform well for determining the number of strides, the walking distance and time. Following a larger study these results may prove this system to be a viable alternative to more expensive gait assessment tools.

Name: Dr. Andrew McDaid
Email: andrew.mcdaid@auckland.ac.nz

HOW PELVIC TILT INFLUENCES MODES OF SPINAL MOTION SEGMENT FAILURE UNDER DIRECT COMPRESSION

Nurul Haiza Sapiee[1], Ashvin Thambyah[1], Peter Roberston[2], Neil Broom[1].
1. Experimental Tissue Mechanics Laboratory, The University of Auckland, New Zealand
2. Department of Orthopaedic Surgery, Auckland City Hospital, New Zealand

INTRODUCTION

Combined flexion and compression of intact ovine lumbar motion segments can result in nuclear material partially penetrating and disrupting the lateral annulus and then tracking intra-annularly towards the posterolateral regions and produce a contained or uncontained herniation. It is suggested that the component of shear resulting from compressing the flexed motion segment has the effect of differentially recruiting the oblique-counteroblique fibre sets in the lateral annulus, overloading one set and giving rise to this localized early lateral disruption. This leads eventually to posterolateral herniation via intra-annular tracking of nucleus [1]. A related study demonstrated that motion segments with defunctioned facets failure at lower compressive loads than those with intact facets, but their herniation pathways are similar [2].

This new study investigated whether increased shear arising from an added component of pelvic tilt would further weaken the lateral annulus an increase the risk of overt herniation in this same annular region.

METHODS

Healthy ovine lumbar spines were obtained fresh, all extraneous soft tissues removed, and separated into motion segments with their facets retained intact (n=26). The motion segments were rehydrated in physiologic saline at 4ºC for 20 hours then mounted in neutral posture in customized stainless steel cups using dental plaster. The segments were then compressed at 40 mm/min while tilted to give a sacral slope angle of 15º. Each test was terminated immediately following the first indication failure - either audible failure or visual herniation. A continuous video recording measured the anterior shear and axial displacements and also captured evidence of failure. Following testing, the segments were fixed in formalin and decalcified to facilitate sectioning and structural analysis of tissue damage.

RESULTS

Fracture of the pars interarticularis occurred in 9 of the 26 segments and was either simultaneous with or immediately following signs of initial disc failure. In 19 of the 26 segments the nuclear material, instead of tracking circumferentially and intra-annularly to the posterolateral annulus, actually extruded directly through the lateral annulus (Figure 1) with a mean failure load of 5.7±0.8kN. The remaining 7 motion segments suffered fracture of the endplate and at a higher mean load 6.3±0.8kN. The high frequency of direct lateral herniations suggests that the increased component of shear arising from the motion segment being compressed in a forward tilted posture renders the lateral annulus more vulnerable to early disruption from whence direct herniation can occur.
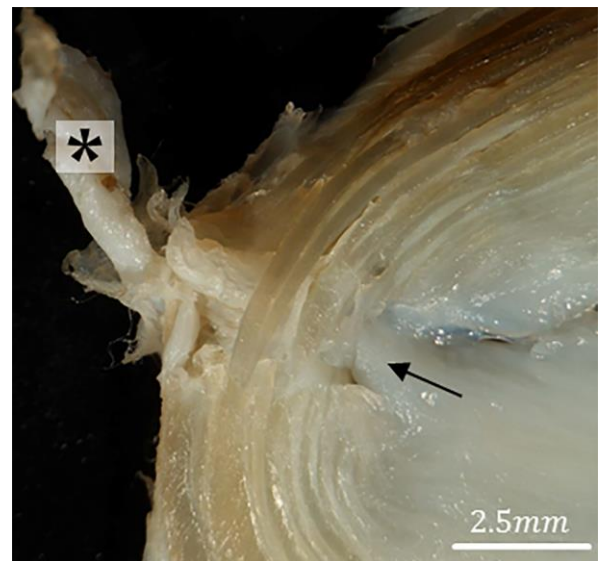

Figure 1. Tranverse section showing penetration of nuclear material through lateral annulus (see arrow) leading to a direct radial extrusion (see asterisk).

CONCLUSIONS

The increased levels of forward shear generated in tilted ovine motion segments when compressed appear to be abnormally damaging to the lateral regions of the disc annulus. This is consistent with the view that shear differentially loads the oblique-counter oblique fibre sets in the lateral annulus making it more vulnerable to early disruption and overt herniation.

ACKNOWLEDGEMENTS

REFERENCES

[1] van Heeswijk VM, et al. Spine 42, 1604-1613, 2017.
[2] Sapiee NH, et al. Spine. Manuscript submitted for publication, 2018.

Speaker: Nurul Haiza Sapiee
Email: nsap465@aucklanduni.ac.nz

THE EFFECTS OF HEEL LIFTS ON LOWER LIMB BIOMECHANICS

Chantel L Rabusin[1,2], Emi Anzai[5], Angela M Evans[1,2], Andrew K Buldt[1,2], Jodie A McClelland[1,3], Hylton B Menz[1,2], Shannon E Munteanu[1,2]

[1] La Trobe Sport and Exercise Medicine Centre, La Trobe University, Melbourne, Victoria, 3086, Australia
[2] Discipline of Podiatry, School of Allied Health, La Trobe University, Melbourne, Victoria, 3086, Australia
[3] Discipline of Physiotherapy, School of Allied Health, La Trobe University, Melbourne, Victoria, 3086, Australia
[4] Department of Human Environmental Sciences, Graduate School of Humanities, Ochanomizu University, 2-1-1 Otsuka, Bunkyo-ku, Tokyo, 112-8610, Japan

INTRODUCTION

Heel lifts are recommended for the management of a number of musculoskeletal conditions including Achilles tendinopathy[1-2], posterior leg muscle strains[3], and plantar heel pain[4-5]. Several studies have investigated the effects of heel lifts on lower limb biomechanics and muscle function on asymptomatic populations, with few studies investigating symptomatic populations[6-12]. Heel lifts have been shown to decrease walking velocity[13], and decrease the ankle joint dorsiflexion angle during running[14] in asymptomatic populations. The effectiveness of heel lifts and the mechanism(s) by which heel lifts may exert their effects remains unclear. The aim of this experimental trial is to investigate the effects of heel lifts on lower limb biomechanics. This information will enable a greater understanding of the therapeutic benefits of heel lifts in treating lower limb musculoskeletal conditions.

METHOD

Thirty volunteers without any current musculoskeletal conditions or known neurological disorders from La Trobe University participated in this study. Ethical approval was obtained from the La Trobe University Human Ethics Committee (S16-35). Verbal and written consent was obtained from all participants prior to participation. Height, weight, leg length, knee and ankle width, inter ASIS distance, ASIS to greater trochanter distance, Foot Posture Index (FPI-6), maximum hallux dorsiflexion angle and maximum ankle dorsiflexion range of motion (lunge test) measurements were obtained. A ten camera three-dimensional motion analysis system (Vicon-MX3, Oxford Metrics Ltd, UK) was used to track 14 mm (diameter) reflective markers attached using double sided tape to anatomical landmarks on each participant. Each participant was asked to walk and run at their natural speed across a 10 m runway in three different conditions: (i) with standardised shoes, (ii) with the addition of 10mm heel lifts and (iii) with the addition of 20 mm heel lifts. The order of conditions was randomised using a computer generated system. Heel lifts were made of hard density Formthotic Formax[TM] foam. Only trials where walking and running speeds were within consistent limits were accepted.

Vicon software were used to process and apply PlugIn Gait and Oxford Foot Model. Lower limb joint angles and moments in the sagittal, coronal and transverse planes were extracted from the three-dimensional motion analysis data for each activity. Only right lower limb data was included in analysis to maintain independence of data. A repeated measures ANOVA was be used to investigate the effects of heel lift on biomechanical outcomes. Any differences will be confirmed with either independent t-tests (between groups) or paired t-test (within group across time).

RESULTS

Ten healthy female and 20 male volunteers (28.43 ± 6.4 years, 1.76 ± 0.80 cm, 73.3 ± 15.0 kg) participated in this study. The average FPI-6, hallux dorsiflexion angle and ankle dorsiflexion range of motion were 3.6 ± 2.5; 67.7 ±20.4◦ and 11.9 ± 3.6 cm respectively. The remaining results from this experimental study will be available and presented at the conference.

Figure 1. Heel lift.

CONCLUSIONS

Three-dimensional motion analysis is essential to provide in depth information of joint movement during walking and running gait. The results of this study will be available at the conference.

REFERENCES

[1] Maclellan, G. Br J Sports Med 15, 117-121, 1981.; [2] Nistor, L. Bone Joint J 63, 394-399, 1981.; [3] Lipton, J. AAO Journal 19, 15-21, 2009.; [4] Black, N. Physiotherapy in Sport 19, 20-22, 1994.; [5] Kogler, G. Foot Ankle Int 22, 433-439, 2001.; [6] Bonanno, D. Gait Posture 33, 385-389, 2011.; [7] His, W. Arch Phys Med Rehabil 80, 801-810, 1999.; [8] Katoh, Y. Foot Ankle Int 3, 227-236, 1983.; [9] Seuser, A. Clin Orthop Relat Res 343,74-80, 1997.; [10] Johanson, M. J Athl Train 41, 159-165, 2006.;[11] Johanson, M. Foot Ankle Int 31, 1014-1020, 2010. ; [12] Wang, C. Clinical Biomechanics 9, 297-302, 1994.; [13] Katoh, Y. Foot Ankle Int 3, 227-236, 1983.; [14] Dixon, S. J Appl Biomech 15, 139-151, 1999.

Speaker: Chantel L Rabusin, Discipline of Podiatry, School of Allied Health, La Trobe University, Melbourne, Victoria, 3086, Australia, Ph +61-3-9479-2166, c.rabusin@latrobe.edu.au

COMBINED EMG-INFORMED NEUROMUSCULOSKELETAL AND SURROGATES OF FINITE ELEMENT MODELS ESTIMATE LOCALISED ACHILLES TENDON STRAIN IN REAL-TIME

Claudio Pizzolato[1], Vickie B. Shim[2], Thor F. Besier[2], Daniel Devaprakash[1], Rod S. Barrett[1], David G. Lloyd[1]
[1] GCORE, Menzies Health Institute Queensland, Griffith University, Gold Coast, Australia
[2]Auckland Bioengineering Institute, University of Auckland, Auckland, New Zealand

INTRODUCTION

Cyclical strain of around 6% helps restore and strengthen damaged tendons (Wang et al. 2015). However, creating exercise programs to train the Achilles tendon within this "sweet spot" is extremely challenging, as different individuals performing the same exercise will elicit different localised tendon strains due to inter-individual variation in musculoskeletal anatomy, neuromechanics, and Achilles tendon morphology and material properties. We present an electromyogram (EMG)-informed neuromusculoskeletal (NMS) of the lower limb combined with a surrogate finite element (FE) model of the Achilles tendon to estimate localised tendon strains during dynamic motor tasks in real-time.

METHOD

One healthy individual was included in this study. A 12-camera motion capture system and an instrumented split belt treadmill were used to collect marker trajectories (200 Hz) and ground reaction forces (1000 Hz) during walking at self-selected speed. Surface EMG were also acquired (2000 Hz) from 16 site on a single leg. A generic OpenSim (Delp et al. 2007) model (gait2392) was linearly scaled to the individual. Joint angles, joint moments, and musculotendon kinematics were subsequently calculated using inverse kinematics, inverse dynamics, and muscle analysis tools in OpenSim.

The Achilles tendon was FE modelled in CMISS (www.cmiss.org) as an incompressible, transversely isotropic hyperelastic material, with 30° twisted fibres, and material properties parameters established from literature (Shim et al. 2014). A partial least squares regression model was implemented in C++ and used to create a surrogate of the FE model able to predict 2048 gauss point von Mises strains from tricep surae muscle forces (Fernandez et al. 2018).

Joint angles, moments, musculotendon kinematics, and surface EMG were used to drive a multiple-degrees of freedom calibrated EMG-informed NMS model (CEINMS) in open-loop (Pizzolato et al. 2015). Muscle forces predicted by CEINMS were used as input for the surrogate model of the Achilles tendon, enabling estimation of 3D localised strains.

Computational speed was evaluated under simulated real-time conditions (Windows 7, i7-6820HQ @ 2.7Hz, 32GB RAM).
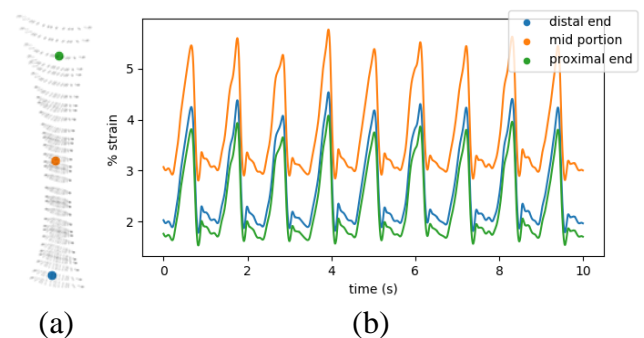
RESULTS

Figure 1 (a) FE model gauss points (grey) and nodes (color) selected for the analysis; (b) real-time von Mises strain estimates during 10 seconds of walking for distal end, mid portion, and proximal end of the Achilles tendon.

The combined CEINMS and surrogate FE models were able to estimate Achilles tendon strain in real-time (Figure 1), with computational time of 1.66 ± 1.10ms per frame, evaluated over 12000 frames.

CONCLUSIONS

This study demonstrated proof-of-concept that localised Achilles tendon 3D strains during gait can be computed in real-time. With current refinement and personalisation underway the approach will be used to provide real-time feedback during tendon training and rehabilitation that target the "sweet spot" required to maximize *in vivo* tendon adaptation (Pizzolato et al. 2017).

REFERENCES

Delp et al. IEEE Trans Biomed Eng 54, 1940-50, 2007
Fernandez et al. CMBBE Imaging Vis (accepted).
Pizzolato et al Front Comput Neurosci 11, 96, 2017
Pizzolato et al Biomech 48, 3929-3936, 2015
Shim et al J Biomech 47, 3598-3604, 2014
Wang et al J Orthop Res 33, 1888-1896, 2015

Claudio Pizzolato c.pizzolato@griffith.edu.au

ABC 11 - Program – DAY 1
Lecture theatre 505-011, Grafton Campus

3rd Dec 2018

| 11.00 am to 12.30 pm

Session Chairs:
Dr Elizabeth Clarke and A/Prof Neils Hammer | **CLINICAL BIOMECHANICS II**
Invited Speaker - A/Prof Sam Veres
Saint Mary's University

On: MEETING THE IN VIVO LOADING REQUIRMENTS OF COLLAGENOUS TISSUES THROUGH STRUCTURAL SPECIALIZATION OVER MULTIPLE LENGTH SCALES: INSIGHTS FROM THE STUDY OF FUNCTIONALLY DISTINCT TENDONS

Scientific Presentations
Can 3-dimensional motion analysis and fuzzy entropy detect movement differences in general movement assessment categories in the normative infant population? – Michelle McGrath (Queensland Health) Effect of ankle push-off haptic biofeedback on lower-limb kinetics and gait symmetry – Duncan Bakke (University of Auckland) Why are certain discs vulnerable to herniation? – Kelly Wade (Ulm University) The influence of feedback and engagement on pedaling performance in stroke patients – Mukesh Soni (University of Melbourne) The use of feedback and video engagement on exercise performance during pedaling - Mukesh Soni (University of Melbourne) |

Can 3-Dimensional Motion Analysis and Fuzzy Entropy detect movement differences in General Movement Assessment Categories in the normative infant population?

Michelle McGrath[1,2,3], Ian Turner[1,3], Hongbo Xie[1,3], Mark Pearcy[1], Robyn Grote[1,2,4], Paul Colditz[2,4]
[1]Queenland University of Technology, Brisbane, Australia. [2]Queensland Health, Brisbane, Australia. [3]ARC Centre of Excellence for Mathematical & Statistical Frontiers (ACEMS), Brisbane, Australia. [4]University of Queensland, Brisbane, Australia

INTRODUCTION

Prechtl's Method on the Qualitative Assessment of General Movement (GMsA) of infants (Darsaklis et al., 2011, Einspieler, 2004) is one method of early prediction of neurodevelopmental outcomes in infants. This movement assessment uses video recordings and the naked eye of the assessor and has established 2 distinct movement classifications (*Writhing* and *Fidgeting*) which occur in healthy infants aged from term to 1 month and 3 months, respectively.

GMsA relies on qualitative classification, resulting in potential intra-, inter- assessor reliability and naked eye errors. A review from Darsaklis et al. (2011) found that there was conflicting evidence that GMsA could accurately predict neurodevelopmental outcomes particularly in cases where the neurological dysfunction was mild. Three-Dimensional Motion Analysis (3DMA) may be a useful tool in measuring small movements that maybe missed in predicting neurodevelopmental outcomes using GMsA's naked eye approach.

Compared to GMsA, 3DMA gives insight in all three planes (sagittal, coronal & transverse) of infant movement without "naked eye" error. Complemented by force plate data, enhanced understanding of the infant postural behaviour can be determined.

METHOD

This novel preliminary study developed an infant 3DMA technical protocol to collect infant movement using the latest 3D motion analysis technology. The collected data (Limb trajectories and ground reaction forces) was used to quantify GMsA movement classifications using a mathematical pattern recognition technique Fuzzy Entropy, in a small cohort of healthy full-term infants.

RESULTS

During the development of the Infant 3DMA protocol, it was found that the optimum placement of markers for the infant biomechanical model, with the least amount of interference from the infant and obstruction from the cameras, were located on the thigh, shin, foot, upper arm, forearm, chest and head segments (Figure 1).

Figure 1: Lightweight reflective markers placed on the infant's head, torso, upper and lower limbs

Fuzzy entropy was found to be a useful mathematical pattern recognition technique to separate movement patterns in the writing and fidgeting datasets especially in the force datasets. It was found that there was a marked decrease in force fuzzy entropy between the writhing and fidgeting data (ANOVA $p \ll 0.05$). It is believed this decrease in entropy is due to the infants' postural stability and control development.

For the trajectory data, the entropy results were inconsistent but there was mostly an increase in entropy, as the infant matured, which indicates a more random movement characteristic indicative of fidgeting behaviour i.e. variable acceleration (Einspieler, 2004). This result would be more conclusive with an increase in the sample size.

CONCLUSIONS

This normative-reference data, along with the developed infant technical protocol and fuzzy entropy, could be used to differentiate between potential normal and abnormal child development and the need for targeted early interventions.

REFERENCES

DARSAKLIS, V., SNIDER, L. M., MAJNEMER, A. & MAZER, B.. *Developmental Medicine & Child Neurology,* 53**,** 896-906.2001

EINSPIELER, C.Mac Keith Press London, UK. 2004

Michelle McGrath

Michelle.McGrath@health.qld.gov.au

EFFECT OF ANKLE PUSH-OFF HAPTIC BIOFEEDBACK ON LOWER-LIMB KINETICS AND GAIT SYMMETRY

Christopher Schenck[1], Duncan Bakke[1], Thor Besier[1,2,3]
[1]Auckland Bioengineering Insititute, University of Auckland, Auckland, New Zealand
[2]Department of Engineering Science, University of Auckland, Auckland, New Zealand
[3]t.besier@auckland.ac.nz

INTRODUCTION
People with stroke experience a significant increase in metabolic cost of walking compared to individuals with normal gait, ascribed to a reduction in ankle push-off and the resulting compensatory work at the hip and contralateral knee [1]. This demonstrates the need for an intervention to encourage use of the ankle plantar flexors to increase ankle power at push-off. However, verbal instruction alone has been shown to be ineffective in altering peak ankle moment or power [2]. Biofeedback (providing feedback on a particular physiological measurement) targeting anterior ground reaction force has been used to effectively modulate peak ankle moment [3]. In this study, we examined the effects of haptic biofeedback driven by real-time estimates of ankle moment in able-bodied subjects.

METHOD
20 able-bodied participants took part in this study (11 male, 9 female, mean age 26). Trials were conducted on a split-belt instrumented treadmill (Bertec, Colombus, OH) to measure ground reaction forces during walking. 8 infra-red motion-capture cameras (Vicon, Oxford, UK) were used to track markers placed on the feet, ankles, legs, pelvis, and torso of each subject.

During the feedback portion of each trial, a LabVIEW VI was used to estimate the instantaneous sagittal-plane moment around the subject's dominant ankle (using the ground reaction force vector, center of pressure, and ankle joint location). At the subject's self-selected comfortable walking speed, this VI provided feedback via a bracelet on the subject's dominant leg containing an Arduino microcontroller, four haptic motors, and a Bluetooth antenna (Figure 1). Two feedback modalities were used, in randomised order for each subject: high and low (aiming to increase and decrease the moment generated around the ankle, respectively).

The feedback was a single-pulse vibration, given if the peak value of the ankle moment during push-off met or exceeded the required threshold (over 10% higher than normal/under 20% lower than normal). A 10-minute washout period of walking with no intervention at the same speed was used between trials to isolate effects of each.

RESULTS
The haptic biofeedback had a significant effect on both ankle moment and power in the targeted leg compared with no-feedback walking. Peak ankle moment and power decreased in the low feedback condition, and peak ankle power increased in the high feedback condition. Preliminary analysis also suggests that feedback modality had an effect on gait symmetry, increasing the absolute percentage difference between peak ankle power for each limb in both cases.

CONCLUSIONS
This study showed that haptic biofeedback is an effective mechanism for altering ankle power in able-bodied individuals, and should be explored for use in stroke populations.

ACKNOWLEDGEMENTS

REFERENCES
[1] Farris DJ et al., *J. Neuroeng Rehab,* **12**:24, 2015.

[2] Lewis CL, Ferris DP, *J .Biomech*, **41**, 2082-2089, 2008.

[3] Genthe K et al., *Top Stroke Rehabil.*, **25**, 186-193, 2018.

SPEAKER INFORMATION
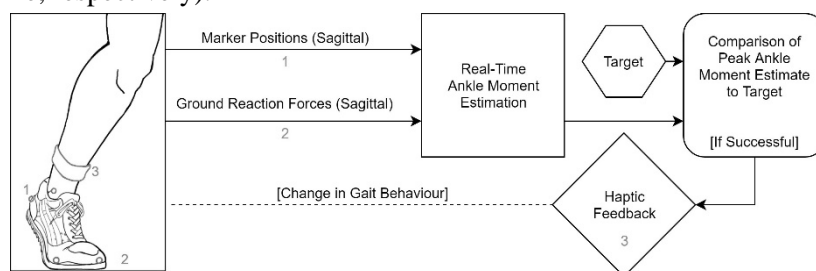Duncan Bakke (dbak576@aucklanduni.ac.nz)

Figure 1: A flow diagram illustrating the system used to provide feedback on estimated ankle moment.

WHY ARE CERTAIN DISCS VULNERABLE TO HERNIATION?

Kelly Wade (1), Nikolaus Berger-Roscher (1), Marija Josipovic (2), Volker Rasche (2), Fabio Galbusera (1), Hans-Joachim Wilke (1)

1. INSTITUTE OF ORTHOPAEDIC RESEARCH AND BIOMECHANICS, ULM UNIVERSITY, ULM, GERMANY; 2. DEPARTMENT OF INTERNAL MEDICINE II, UNIVERSITY HOSPITAL ULM, ULM, GERMANY

INTRODUCTION

Clinically, disc herniation results from annular failure or endplate junction failure [1]. These cases have been reproduced *in vitro* [2], and it is known that both posture and loading rate influence the nature of herniation [3]. However, it has not been possible to accurately assess disc structure prior to testing and the effects of components of complex loading have also not been studied in detail. Therefore, the goal of this study was to investigate the role of different loading combinations and disc structure itself in the process of disc failure. Our hypothesis was that certain structural features may be correlated with certain modes of herniation.

METHOD

Thirty lumbar spinal segments from mature ewes (3-5 years old) were subjected to a combination of four loading conditions (0-12° flexion, 0-9° lateral bending, 0-4° axial rotation, 0-800 N axial compression) for 1000 loading cycles at 2 Hz in a recently developed dynamic 6-DOF disc loading simulator. One group was subjected to all loading conditions and the other four groups had one condition omitted to allow identification of potential effects of the loading conditions. Macroscopic changes of the posterior part of the disc were recorded by video during testing. Prior to and after testing the discs were scanned with ultra-high field MRI (11.7 T) and µCT. They were then fixed and decalcified to enable cryosectioning, then analyzed microstructurally with light microscopy.

RESULTS

Ten discs suffered annular failure, with four of these involving subligamentous herniation of inner disc material and the remaining protrusion of inner disc material into the outer annulus as judged by examination of the high resolution MRI images. All discs that herniated contained distinctive irregularities in the posterior mid-inner annulus visible in pretest MRI images as can be seen in Figure 1. Microstructural investigation revealed that the mid-outer annular-endplate junction had failed in all herniated discs.
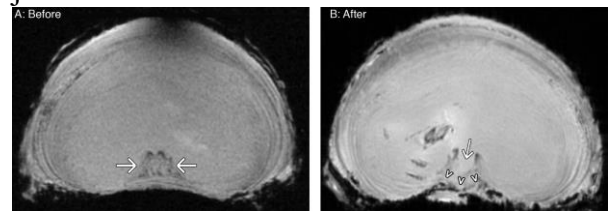

Figure 1: Transverse 11.7T MRI section through an ovine disc prior to testing (A) Arrows indicate irregularities. Following testing (B) inner disc material can be seen to have been extruded through this region as indicated by the arrow and largely contained by the posterior ligament as indicated by the arrowheads.

CONCLUSIONS

These results indicate that the distinctive irregularities in the lamellar structure are responsible for annular failure and herniation under these loading conditions. They appear to act as initiation sites for herniation since inner disc material extrudes through them when the disc is overloaded regardless of the posture applied. The failure of the posterior mid-outer annulus at the endplate junction is likely a consequence of the compromised annulus being unable to contain the pressure generated within the nucleus.

This study indicates that experimental MRI imaging may be able to detect discs vulnerable to herniation, at least in the ovine samples used in the present study. It may thus be possible in the future to develop clinical imaging techniques to identify patients at risk of herniation.

REFERENCES

1. Rajasekaran S, Bajaj N, Tubaki V, Kanna RM, Shetty AP. Spine. 2013;38(17):1491-500.
2. Wilke, H.-J., A. Kienle, S. Maile, V. Rasche and N. Berger-Roscher (2016) European Spine Journal 25(5): 1363-1372.
3. Wade KR, Robertson, P.A., Thambyah, A., Broom, N.D. Spine. 2015;40(12):891-901.

Presenter: Kelly Wade; wadekellyr@gmail.com

THE INFLUENCE OF FEEDBACK AND ENGAGEMENT ON PEDALING PERFORMANCE IN STROKE PATIENTS

[1,2]Mukesh Soni, [2]Tissa Wijeratne, [2]Nihara Abdul Rasheed and [1]David C. Ackland
[1]Department of Biomedical Engineering, The University of Melbourne, Melbourne, Victoria
[2]Department of Neurology, Western Health Sunshine Hospital, Melbourne, Victoria
email: dackland@unimelb.edu.au

INTRODUCTION
Pedaling using an exercise bicycle is a popular exercise to improve aerobic capacity and a safe home-based therapy for rehabilitation of stroke patients with affected lower limbs. However, the repetitive nature of pedaling is associated with poor motivation, exercise adherence and lack of perceived self-efficacy which limits its usage by the patients [1]. Use of extrinsic feedback on exercise performance and audio-visual stimuli in isolation has been reported to make exercise enjoyable and improve exercise compliance, perceived exertion as well as recovery of motor function among stroke patients [2]. However, the influence of visual feedback and performance linked video engagement on exercise performance and physiology is not well understood. The aim of this study was to assess the influence of both feedback and engagement on pedaling performance and cardiopulmonary output, including blood oxygen saturation (Sp02) and heart rate (HR). We hypothesize that video-engagement and exercise parameter feedback during pedaling will reduce fatigue by mitigating exercise-related changes in Sp02 and HR.

METHOD
Thirteen stroke patients (mean age: 64 years, range: 25-78 years) with mild lower limb disability and 18 healthy controls (mean age: 27.7 years, range: 25-41 years) were recruited. All subjects were asked to pedal and maintain a specified target speed on a custom-designed stationary bicycle. A screen visible to the participant was capable of displaying pedaling exercise details including current and target speed (feedback), as well as a video (engagement) during pedaling. Participants performed six sessions of 15-minutes pedaling at low (60 RPM) and high speeds (100 RPM), with different combinations of intervention type (baseline pedaling, pedaling with feedback, pedaling with engagement). HR and SpO2 were recorded along with the pedaling parameters.

A 3-way, mixed Analysis of Variance was used to assess the effect of intervention type, pedaling speed and participant type (stroke or controls) on HR, SpO2, pedaling workload and speed parameters. Post-hoc tests were undertaken using paired t-tests and Games-Howell tests for groups with un-equal variances. Level of significance was defined as $p \leq 0.05$.

RESULTS
For stroke patients, the average reduction in SpO2 increased with feedback and engagement, relative to baseline or pedaling without intervention (Table 1). HR reduced in the stroke patients with visual feedback and video engagement during pedaling, relative to baseline pedaling; however, the influence of engagement on reduced HR relative to feedback was more pronounced in stroke patients than in healthy controls during high-speed pedaling (HR reduction: 5.8 beats/min in patient vs 4.9 beats/min in healthy control). The pedaling induced workload changes were higher for the stroke patients than in healthy controls. Pedaling performance, in terms of absolute speed deviation and its variability, improved significantly ($p<0.006$) in stroke patients with the application of feedback and engagement, but only during low-speed pedaling.

CONCLUSIONS
This study demonstrated that visual feedback and video engagement have the potential to improve exercise performance and HR workload experience in stroke patients for low-to-moderate intensity pedaling exercises. The results have implications for prescription of targeted exercise therapies and post-stroke rehabilitation using pedaling in the home.

REFERENCES
1. Simpson L, et al., Int. J. Ther. Rehabil. 18(9):520-530, 2011
2. Kamps A, et al., Neurol Rehabil. 11(5): 1-12, 2005

Table 1: Comparison of means for SpO2, HR and exercise parameters during pedaling at low and high speeds. Mean difference and their significance (p value) are given. One asterisk indicates p <= 0.05, two asterisks indicate p<=0.01, while three asterisks indicate p<=0.001.

| | | Healthy Subjects | | | | | | Stroke Patients | | | | | |
| | | Feedback vs Baseline | | Engagement vs Baseline | | Engagement vs Feedback | | Feedback vs Baseline | | Engagement vs Baseline | | Engagement vs Feedback | |
Exercise Parameters	Pedaling Speed	Mean Diff	p value	Mean Diff	p value	Mean Diff	p value	Mean Diff	p value	Mean Diff	p value	Mean Diff	p value
SpO2: Average Reduction	Low	0.371	0.078	0.333	0.126	-0.037	0.880	-0.128	0.718	-0.332	0.441	-0.205	0.676
	High	0.093	0.613	0.463	0.004 **	0.370	0.109	-0.283	0.687	-0.153	0.780	0.130	0.793
HR: Average Increase	Low	-1.351	0.622	-5.612	0.129	-4.261	0.184	-1.769	0.168	-1.025	0.531	0.745	0.529
	High	0.816	0.817	-4.148	0.180	-4.964	0.111	2.025	0.377	-3.798	0.353	-5.822	0.181
Absolute Speed-deviation	Low	-2.996	0.028 *	-3.389	0.010 **	-0.393	0.723	-1.777	0.014 *	-2.444	0.006 **	-0.667	0.175
	High	-3.085	0.002 **	-2.187	0.007 **	0.898	0.383	0.174	0.868	0.035	0.954	-0.140	0.884
COV (Abs. Speed-deviation)	Low	24.177	0.002 **	25.396	0.002 **	1.219	0.950	16.714	0.001 ***	20.880	0.000 ***	4.166	0.179
	High	23.025	0.000 ***	13.911	0.017 *	-9.114	0.033 *	3.815	0.402	1.840	0.669	-1.975	0.695

THE USE OF FEEDBACK AND VIDEO ENGAGEMENT ON EXERCISE PERFORMANCE DURING PEDALING

[1,2]Mukesh Soni, [2]Tissa Wijeratne and [1]David C. Ackland
[1]Department of Biomedical Engineering, The University of Melbourne, Melbourne, Victoria
[2]Department of Neurology, Western Health Sunshine Hospital, Melbourne, Victoria
email: dackland@unimelb.edu.au

INTRODUCTION

Cycling has been used in lower-limb rehabilitation following orthopaedic surgery to improve aerobic capacity and cardiopulmonary function. Use of visual feedback on exercise performance, music and video engagement has been reported to improve exercise compliance, perceived exertion as well as motor relearning in people with lower limb weakness as this distracts from fatigue associated with exercise [1,2]. However, the effects of both activity performance feedback and video engagement on exercise performance remains poorly understood. The aim of the present study was therefore to develop a novel pedaling device that provides real-time exercise performance feedback as well as video engagement and assess the influence of both this feedback and engagement on pedaling performance and exercise physiology parameters including blood oxygen saturation (Sp02) and heart rate (HR). We hypothesized that provision of video-engagement and exercise parameter feedback during pedaling will reduce fatigue by mitigating exercise induced changes in Sp02 and heart rate.

METHOD

Eighteen healthy participants (mean age: 27.7 years, range: 25-41 years) attended an exercise monitoring study where they pedaled on a custom-designed stationary exercise bicycle that displays pedaling data output (feedback) and also allowed the user to watch a video simultaneously (engagement). Participants pedaled for 6 sessions of 15-minutes each with different combinations of intervention type (baseline pedaling, feedback, and engagement) and were requested to pedal at two contrasting speeds: 60 RPM and 100 RPM. HR and SpO2 were simultaneously recorded along with the current speed and target speed.

A 2-way Analysis of Variance (ANOVA) was used to assess the effect of intervention type and pedaling speed on HR, SpO2, pedaling workload and speed parameters. Post-hoc tests were undertaken using paired t-tests and Games-Howell tests for groups with un-equal variances. Level of significance was defined as $p \le 0.05$.

RESULTS

During high-speed pedaling, engagement resulted in smaller reduction, relative to baseline, in average SpO2 (mean difference = 0.296%, p=0.035) and post-exercise SpO2 change from resting value (mean difference = 0.611%, p=0.007) (Table 1). Visual feedback resulted in a reduction of 6.259 beats per minute (p=0.047) in mean HR relative to baseline during low-speed pedaling. Pedaling performance, in terms of absolute speed deviation from target and variability in pedaling speed, improved significantly with feedback (p<0.008) and engagement, relative to baseline.

CONCLUSIONS

This study demonstrated that visual feedback during stationary pedaling has the effect of improving targeted pedaling performance, while the addition of video engagement during pedaling has the potential to reduce the burden of repetitive pedaling on cardiopulmonary performance. The results have implications for prescription of targeted exercise therapies and rehabilitation using pedaling in the home.

REFERENCES

1. Kamps A, et al., Neurol Rehabil. 11(5): 1-12, 2005.
2. Ortis LC, et al., Psicothema. 19(2): 250-255, 2007.

Table 1: Comparison of mean SpO2, HR and exercise parameters during pedaling at low and high speeds. Data are compared with the use of feedback and engagement against baseline pedaling. Mean difference and p-values are given. One asterisk indicates p <= 0.05, two asterisks indicate p<=0.01, while three asterisks indicate p<=0.001.

	Low Speed						High Speed					
	Feedback Vs Baseline		Engagement Vs Baseline		Engagement Vs Feedback		Feedback Vs Baseline		Engagement Vs Baseline		Engagement Vs Feedback	
	Mean Diff.	p value	Mean Diff.	p value	Mean Diff.	p value	Mean Diff.	p value	Mean Diff.	p value	Mean Diff.	p value
SpO2: Session Mean	-0.018	0.892	0.000	1.000	0.018	0.914	0.315	0.063	0.296	0.035 *	-0.019	0.918
Change at 15-minutes	0.333	0.138	0.500	0.015 *	0.167	0.483	0.222	0.331	0.611	0.007 **	0.389	0.130
HR: Session Mean	-6.295	0.047 *	-5.778	0.072	0.517	0.851	1.483	0.646	-6.092	0.097	-7.575	0.018 *
Change at 15-Minutes	1.167	0.725	-7.056	0.085	-8.222	0.050 *	0.111	0.979	-4.722	0.241	-4.833	0.168
Speed: Absoute Deviation	-2.996	0.027 *	-3.389	0.008 **	-0.393	0.722	-3.085	0.002 **	-2.187	0.007 **	0.898	0.383
COV (Speed Variability)	-0.441	0.166	-0.558	0.083	-0.117	0.687	-0.986	0.037 *	-0.860	0.034 *	0.127	0.582

ABC 11 - Program – DAY 1
Lecture theatre 505-011, Grafton Campus

3rd Dec 2018

1.30 pm to 3.00 pm Session Chairs: A/Prof Thor Besier and Dr Yanxin Yang	**SPORTS BIOMECHANICS** **Invited Speaker - Professor Patria Hume** Auckland University of Technology On: HOW SPORTS BIOMECHANICS HELPS IMPROVE PERFORMANCE AND REDUCE RISK **Scientific Presentations** - Characterizing stress patterns in the brains after traumatic brain injury– Vickie Shim (University of Auckland) - Inter- and intra-day reliability of common injury screening measures in rugby league is variable – Tim Doyle (Macquarie University) - Foot pronation is associated with increased knee joint loading rate and adduction after long distance running – Justin Fernandez (University of Auckland) - Lower limb impact accelerations vary with sensor placement – Daniel Glassbrook (Macquarie University) - Stride length, thorax and pelvic positioning during lawn bowls deliveries – Jodie McCelland (La Trobe University)

CHARACTERIZING STRESS PATTERNS IN THE BRAINS AFTER TRAUMATIC BRAIN INJURY

Vickie Shim[1], Mike Dragunow[2] & Shaofan Li[3]
[1]Auckland Bioengineering Institute, University of Auckland
**[2]Centre for Brain Research, University of Auckland**
[3]Department of Civil and Environmental Engineering, UC Berkeley

INTRODUCTION

Traumatic brain injury (TBI) is a major public health challenge that is on course to become the third leading cause of death worldwide by 2020(1). As yet, there is not even a clear and objective injury threshold for mTBI let alone medications that can reduce brain damage or promote brain repair(2). Numerous studies on TBI have been conducted in the past using animal models, cell cultures and computational models. Yet, we still do not even have a capability to objectively identify injury threshold for brain concussion. One main reason is that a clear link between the mechanical factors of the concussion and subsequent downstream cellular events have not been established, especially in humans. We do not know how the mechanical energy from concussion is transferred to the brain and then to the cellular and vessel network within the brain causing damages in the tissue. We will address this need by combining state-of-the-art neuroscience with high fidelity multi-scale computational models of the brain.

METHOD

The existing human brain model is from the International Union of Physiological Society (IUPS) Physiome Project (3), which contains the scalp, skull and the brain. This model has been further developed into a 3D model with tissue anisotropy of the white matter, an important mechanical feature of the brain(4) by embedding the fibre orientation of the white matter to the model. We used the microstructurally based material coordinate system in our FE software (5) (www,opencmiss.org, freely available for academic use), which has been used to describe anisotropy of various tissue such as the heart and skeletal muscles.

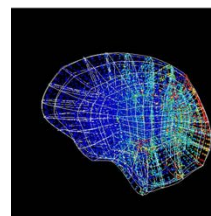Head model   Brain model   Fibres of the white matter
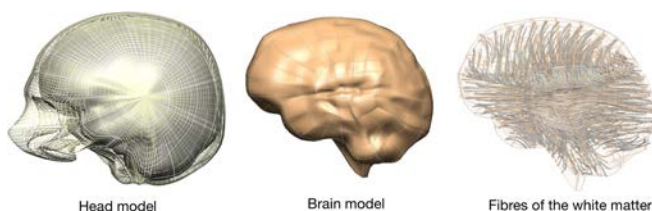
A parametric study was performed with this model to identify the pattern of damage in the brain of rugby players. The linear and angular accelerations 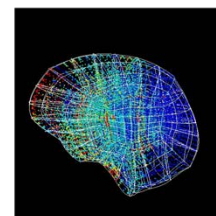at the time of impact during rugby games or practices were obtained from wearable sensors (measured by CSx, an Auckland based concussion sensor company, www.csx.co.nz). This was applied to a parameterized model of the brain and the resulting stress pattern was observed.
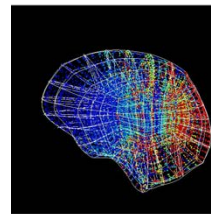
RESULTS

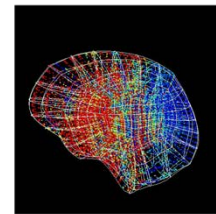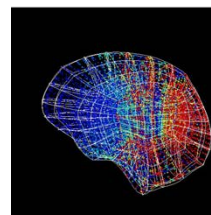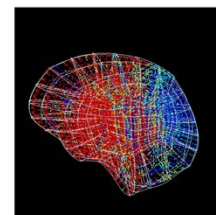Two brain impact scenarios - frontal and occipital impacts based on the previously measured head kinematics data (6) were used to simulate stress propagation after impact. to the type of loading as well as the internal tissue structure. This will be further investigated using a machine learning algorithm to characterize the pattern of damage after head impact more fully.

Occiptal Impact   Frontal Impact

t=15ms   t=15ms

t=30ms   t=30ms

t=45ms   t=45ms

REFERENCES

1.Young et al. Lancet Neurol. 2010;9(4):331.
2. Sharp DJ, Jenkins PO. Pract Neurol. 2015;15(3):172-86.
3. Hunter PJ, Borg TK. Nature reviews Molecular cell biology. 2003;4(3):237-43.
4. Giordano C, Cloots RJ, van Dommelen JA, Kleiven S. J Biomech. 2014;47(5):1052-9.
5. Shim VB, Besier TF, Lloyd DG, Mithraratne K, Fernandez JF. Biomech Model Mechanobiol. 2016;15(1):195-204.

v.shim@auckland.ac.nz

INTER- AND INTRA-DAY RELIABILITY OF COMMON INJURY SCREENING MEASURES IN RUGBY LEAGUE IS VARIABLE.

[1] Doyle, Tim L. A., [2] Devlin, P., [2] Wade, J., [2] Farrah, E., [1] Cramer, M., and [1] Ollerton, L.
[1] Faculty of Medicine and Health Sciences, Macquarie University, Sydney, NSW, Australia.
[2] South Sydney Football Club, Sydney, NSW, Australia.

INTRODUCTION
Rugby league requires muscular strength, power, speed, agility, and aerobic capacity.[1] As such, pre-season screening of athletes is commonly performed in an attempt to identify risk factors of musculo-skeletal injury.[2] Commonly, tests are chosen based on clinical experience, but may lack suitable determination of their reliability and/or validity. Consequently, the aim of this study was to assess the inter- and intra-day reliability of the knee-to-wall, adductor groin squeeze, bent knee fallout, sit and reach, and handgrip strength tests in professional rugby league players.

METHOD
Participants: 27 male professional rugby league players provided written informed consent (age: 24.6 (4.1) yrs, mass: 1003. (10.5) kg, height: 1.86 (0.07) m)) This project has ethical approval from Macquarie University HREC (no. 5201600790).

Five tests were repeated twice in one day and one week apart. The tests used were: knee to wall, adductor squeeze test, bent knee fallout, sit and reach test, and hand dynamometer grip strength test.

Two-tailed paired t-tests ($\alpha=0.05$) were performed to compare the differences between trials on the same day and trials one week apart. Intraclass correlation coefficients (ICC model 3.1) were calculated to examine test-retest repeatability. ICC criteria were: values less than 0.5, between 0.5 and 0.75, between 0.75 and 0.9, and greater than 0.9 are indicative of poor, moderate, good, and excellent week-to-week repeatability, respectively. ICC data are presented as ICC [95%CI]. The technical error of measurement (TEM) was calculated to express measurement error and describe the precision of the tests.

RESULTS
Generally, the knee to wall and sit and reach tests demonstrated acceptable reliability within and across days. The adductor squeeze test and bent knee fallout tests demonstrated unacceptable levels of reliability when considering both inter- and intra-day reliability. Finally hand dynamometer grip strength test had good inter-day reliability but varied intra-day depending on hand dominance, table 1.

CONCLUSIONS
Knee to wall, sit and reach, and dominant bent knee fallout and handgrip strength demonstrated acceptable reliability in professional rugby league players. Poor reliability of the remaining tests suggests clinicians should exercise caution when using these tests for injury screening in this population.

REFERENCES
1. Br J Sports Med., 44, i5, 2010.
2. Br J Sports Med., 32, 68–70, 1998
Speaker: Dr. Tim Doyle, tim.doyle@mq.edu.au

Table 1: Inter- and Inra-day reliability of musculoskeletal screening tests

Test	Intra-Day			Inter-Day		
	ICC (95%CI)	TEM	TEM %	ICC (95%CI)	TEM	TEM %
Knee to wall *(cm)*						
Dominant leg	0.93 (0.84-0.97)	0.75	6.33	0.95 (0.89-0.98)	0.60	5.0
Non-dominant leg	0.83 (0.63-0.92)	0.92	7.91	0.92 (0.81-0.97)	0.61	5.2
Adductor squeeze *(mmHg)*	0.37 (-0.03-0.67)	25.53	10.53	0.78 (0.55-0.90)	14.81	5.9
Bent knee fallout[b] (*cm*)						
Dominant leg	0.54 (0.17-0.77)	2.74	24.34	0.82 (0.59-0.92)	1.85	15.9
Non-dominant leg	0.51 (0.13-0.76)	2.97	27.56	0.48 (0.07-0.75)	2.97	24.0
Sit and reach[c] *(cm)*	0.92 (0.82-0.96)	1.51	27.62	0.95 (0.89-0.98)	1.18	20.9
Grip strength *(kg)*						
Dominant hand	0.83 (0.60-0.93)	4.46	8.88	0.91 (0.79-0.96)	3.42	6.5
Non-dominant hand	0.42 (-0.02-0.73)	5.44	10.31	0.64 (0.29-0.84)	5.09	9.6

ICC = Intraclass coefficient, CI = Confidence intervals, TEM = Technical error measurement, TEM% = Technical error measurement expressed as a percentage.

FOOT PRONATION IS ASSOCIATED WITH INCREASED KNEE JOINT LOADING RATE AND ADDUCTION AFTER LONG DISTANCE RUNNING

Qichang Mei, Yaodong Gu, Liangliang Xiang, Vickie Shim, Justin Fernandez
Auckland Bioengineering Institute, University of Auckland
Research Academy of Grand Health Interdisciplinary, Ningbo University

INTRODUCTION

Long distance running has been increasing in popularity and participation, however, is also associated with increased injury rates, especially the knee joint [1]. Previous studies have reported foot morphology changes and plantar pressure redistribution associated with long distance running [2]. However, less information has been reported about foot posture changes during long distance running, and the associated changes in knee joint loading. This study investigates changes in foot posture after 5km running and the associated changes in the knee adduction moment and knee joint force.

METHOD

Twenty recreational runners participated in this study (ethics approved by Ningbo University), with each participant having their foot posture measured using a Foot Posture Index (FPI) (Figure 1). A Standard motion analysis (Vicon) was also conducted before and after a 5km treadmill run. An OpenSIM musculoskeletal model (Gait Model2392) was modified to predict the knee joint adduction/abduction moment and joint reaction force, and was scaled using static trials based on each participants' anthropometry and body mass. Inverse kinematics and inverse dynamics was performed using OpenSim 3.3.

RESULTS

The foot posture index (FPI) score showed the pronation increased significantly after 5km treadmill running, presenting with 0.75±2.82 (Pre 5km) vs 5.1±2.99 (Post 5km), with p<0.05. Significant increases in the knee joint force loading rate post 5km were also observed. The increased FPI (pronation) score was mildly correlated to the knee joint loading rate (R^2~0.21) pre 5km and increased post 5km (R^2~0.31). The FPI (pronation) score revealed better correlation to the knee adduction moment pre 5km (R^2~0.33) increasing post 5km (R^2~0.45).

Figure 2 caption below. Linear regression analysis between FPI and loading rate of knee joint reaction force (left) and FPI and knee adduction moment (right).

CONCLUSIONS

This study revealed that increased foot pronation may be a contributory factor to increased knee joint force loading rates and knee adduction moments. Footwear design or bracing that reduces pronation in long distance running may have a beneficial role.

REFERENCES

1. van Gent et al. *Br J Sport Med*, 40(4), 16-29, 2007.

2. Mei et al. Acta of Bioeng and Biomech, In press, 2018.

Presenting author: A/Prof. Justin Fernandez

Email: j.fenandez@auckland.ac.nz

Neutral   Pronated
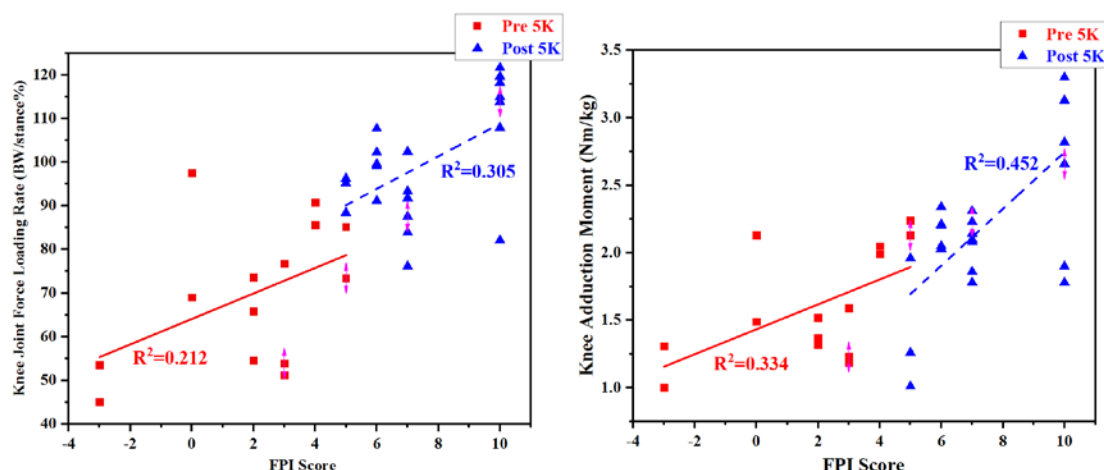
LOWER LIMB IMPACT ACCELERATIONS VARY WITH SENSOR PLACEMENT

Daniel J. Glassbrook[1], Joel T. Fuller[1], Jacqueline A. Alderson[2], and Tim L. A. Doyle[1]
[1] Faculty of Medicine and Health Sciences, Macquarie University, Sydney, Australia
[2] Faculty of Science, The University of Western Australia, Perth, Australia

INTRODUCTION

Accelerometers are often placed on the medial border of the tibia, just above the medial malleolus, to measure accelerations associated with running (Crowell et al., 2011; Raper et al., 2018). For example, peak resultant accelerations (PRA) at the distal tibia can provide an indication of lower-limb loading, and associated risk of running injury (Milner et al., 2006). However, it may not always be feasible to place an accelerometer on the medial border of the tibia, or elsewhere on the lower-limb. For example, in contact sports, where sensors attached to the skin may cause injury if impacted. In this case, the dorsum of the foot (shoe laces) may be a feasible option.

METHOD

Fifteen recreationally active participants (Male $n = 9$, 23.9 ± 3.6 years, 1.77 ± 0.05 m, 78.3 ± 12.0 kg; Female $n = 6$, 27.3 ± 6.0 years, 1.69 ± 0.05 m, 66.3 ± 10.7 kg) volunteered to participate in this study. This study was approved by the Macquarie University Human Research Ethics Committee (protocol: 5201700532). Written informed consent was provided by each participant prior to participation.

Participants completed three familiarisation and one test session. The sprint protocol was performed on a non-motorised treadmill (Force 3, Woodway USA, Inc., Waukesha, WI, USA). After a standardised dynamic warm up of two minutes of steady state running at 50-60% self-perceived maximal effort (%Max) followed by 30-60 second rest, five x 15-s sprints (70, 80, 90, 100 and 100%Max, respectively) were completed. A 60-s active recovery (60%Max) was included immediately before and after each sprint effort.

Four accelerometers (iMeasureU, Auckland, New Zealand) were used to measure accelerations in three axes (x, y, and z) at 500 Hz. One accelerometer was attached distally to each tibia, just above the medial malleolus (TIB_{Left} and TIB_{Right}). The remaining two accelerometers were attached to the laces of each participants' running shoe by threading the laces through the sensor and securing with rigid sports tape (DOR_{Left} and DOR_{Right}).

Analysis of step-by-step acceleration data for each accelerometer was performed using proprietary software (IMU_Step, version 1.0, iMeasureU, Auckland, New Zealand). The variable of interest was the PRA during the best 100% sprint. The manufacturer's software is designed for moderate speed running and has not been optimised for high-speed running. The best 100% sprint was determined by qualitative visual inspection. Paired t-tests were used to assess any systematic bias between sensor locations. Pearson's correlations were used to determine the association between PRA data from different sensor locations.

RESULTS

Mean PRA results are presented in Table 1. Large differences were observed between sensor locations on the left (t(14) = -6.74, $p < 0.05$), and right sides (t(14) = -6.93, $p < 0.05$). The TIB_{Left} was positively correlated to DOR_{Left} (r = 0.51, $p = 0.054$). The TIB_{Right} was positively correlated to DOR_{Right} (r = 0.39, $p = 0.152$).

Table 1. Mean ± standard deviation peak resultant acceleration results for each sensor placement.

Tibia (L)	Dorsum (L)	Tibia (R)	Dorsum (R)
131.0 ± 19.8*	176.9 ± 30.1*	129.5 ± 25.6^	176.5 ± 21.6^

L, Left; R, Right. * $p < 0.05$ Tibia (L) vs Dorsum (L); ^ $p < 0.05$ Tibia (R) vs Dorsum (R).

CONCLUSIONS

The results of this study suggest that accelerometers placed on the dorsum of the foot detect larger PRAs when compared to the conventional placement on the distal medial tibia. Therefore, previous findings that are based on tibial accelerometers cannot be directly applied to dorsal foot accelerometers. Future research should investigate the relationship between dorsal foot accelerometers and injury risk because it is not always possible for athletes to wear sensors on the tibia.

REFERENCES

Crowell, H. P. Et Al. Clin Biomech. 26(1), 78-83, 2011.
Milner, E. Et Al. Med Sci Sports Exerc. 38(2), 323-328, 2006.
Raper, D. P. Et Al. J Sci Med Sport. 21(1), 84-88, 2018.
Speaker Information: Daniel Glassbrook, daniel.glassbrook@mq.edu.au

STRIDE LENGTH, THORAX AND PELVIC POSITIONING DURING LAWN BOWLS DELIVERIES

Samantha Birse[1], Kate Webster[1], Jodie McClelland[1], and Kane Middleton[1]
[1]School of Allied Health, La Trobe University, Melbourne, Australia

INTRODUCTION

Success in the sport of lawn bowls is determined by an athlete's ability to roll a biased bowl accurately towards a target up to 37m away. With a lack of research investigating lawn bowling technique, technical coaching is typically based on anecdotal evidence and individual athlete preference. General recommendations for lawn bowling technique have been proposed [1] but have failed to distinguish techniques that are specific to the forehand or backhand deliveries, or how technique may change across an array of bowling lengths. As previous research has found that older lawn bowls players had better balance when releasing the bowl than matched controls [2], this increased stability may also lead to more accurately deliveries. The position of the thorax and pelvis is then likely to have implications for specific training for different conditions. Therefore, the aim of this study was to compare the differences in thorax and pelvic kinematics, in addition to stride length between different lawn bowling conditions.

METHOD

Nineteen male ($n = 12$) and female ($n = 7$) (age 28.5 ± 7.6 years, height 175.4 ± 9.9 cm, mass 82.4 ± 21.0 kg) national and international representative lawn bowlers were assessed during four different bowling conditions: (i) forehand delivery to a jack placed 23m from the athlete (FH Short); (ii) FH delivery to a jack placed 27m from the athlete (Long); (iii) backhand (BH) delivery to a short jack; and (iv) BH delivery to a long placed jack, where a forehand delivery was defined when the bowls trajectory apex was on the same side as the bowling arm. Before proceeding to the next condition, participants needed to have five deliveries resulting within 60cm of the Jack. Thorax and pelvis kinematics were collected by a 20 camera motion capture system throughout the delivery with kinematics being observed at the time of bowl release. Significant between condition differences ($P<0.01$) were compared using a two-way repeated measures analysis of variance with two factors; delivery type (FH/BH) and bowling length.

RESULTS

There was no main effect of bowling length, nor significant interaction. A significant main effect ($P<0.001$) of delivery hand for all pelvic and thorax kinematics as well as stride length was shown. Pairwise comparisons showed that during BH deliveries athletes had significantly greater anterior pelvic tilt, less ipsilateral pelvic hitch, greater ipsilateral pelvic rotation, as well as greater thorax flexion, less contralateral flexion, greater ipsilateral thorax rotation, and longer stride (Table 1) compared to bowling on the FH.

CONCLUSIONS

Clear differences between FH and BH deliveries were observed for these different conditions, however the athletes did not change their stride length, thorax or pelvic position to adapt to different between bowling lengths when releasing the bowl. Therefore, coaching techniques that are specific to FH and BH may be warranted to improve performance.

REFERENCES

[1] Judson, R. Lawn Bowls Coaching, 2003

[2] Sayers, M. G. et al. J Aging Phys Act 23, 34-39, 2015.

Samantha Birse
S.Birse@latrobe.edu.au

Table 1. Mean (±SD) of thorax and pelvic angles (°), as well as stride length (cm) for FH and BH deliveries at both 23m (short) and 27m (long) bowling lengths.

Kinematic Variable	Bowling Conditions				FH/BH Effect *P*-Value	Length Effect *P*-Value	Interaction *P*-Value
	BH Short	BH long	FH short	FH Long			
Pelvis Anterior Tilt	38.7 ± 10.8	38.5 ± 11.1	35.4 ± 11.7	34.2 ± 12.6	<0.001**	0.22	0.08
Pelvis Contra Drop	11.8 ± 6.5	11.9 ± 6.5	18.7 ± 7.6	19.0 ± 7.4	<0.001**	0.59	0.57
Pelvis Ipsilateral Rot	11.0 ± 8.2	11.0 ± 7.4	2.8 ± 8.4	2.0 ± 8.0	<0.001**	0.26	0.11
Thorax Flex	68.8 ± 7.0	69.7 ± 7.7	65.8 ± 7.4	66.4 ± 8.6	<0.001**	0.04	0.38
Thorax Contra Flex	15.1 ± 15.2	14.7 ± 14.9	24.9 ± 18.4	24.5 ± 18.2	<0.001**	0.21	0.99
Thorax Ipsilateral Rot	25.9 ± 10.7	26.0 ± 10.8	21.7 ± 8.8	22.2 ± 8.6	<0.001**	0.53	0.51
Stride Length	131.0 ± 23.7	129.4 ± 22.9	76.1 ± 16.3	75.6 ± 18.5	<0.001**	0.33	0.60

** significant main effect P<0.01

ABC 11 - Program – DAY 1
Lecture theatre 505-011, Grafton Campus

3rd Dec 2018	
3.30 pm to 5.00 pm Session Chairs: Dr Hossein Mokhtarzadeh and Dr Eng Kuan Moo	**ORTHOPAEDIC BIOMECHANICS** **Invited Speaker - Dr Marcos Domingos** University of Manchester On: 3D BIOPRINTING: CURRENT AND FUTURE TRENDS IN SKELETAL TISSUE REGENERATION **Scientific Presentations** - Understanding the scaphoid kinematics after sectioning of scapholunate ligament - Ita Suzana Mat Jais (Singapore General Hospital) - Exploring lesser known mechanisms of structural failure in mechanically-induced disc herniations - Vonne van Heeswijk (University of Auckland) - Effects of lower limb anthropometry on gait stability - Sandro Mihradi (Institut Teknologi Bandung) - Bone microarchitecture damage due to press-fit femoral knee implantation quantified using HR-pQCT and digital volume correlation- Egon Perelli (Flinders University) Comparing Cartilage thickness and subchondral bone microarchitecture in varus- and valgus-aligned osteoarthritic tibiae with controls – Sophie Rapagna (Flinders University)

Understanding the scaphoid kinematics after sectioning of scapholunate ligament

Ita Suzana Mat Jais[1], Alyssa LiYu Toh[1], Yoke Rung Wong[1]
[1] Biomechanics Laboratory, Singapore General Hospital, Singapore

INTRODUCTION

The primary function of ligaments in wrist motion is to maintain normal, anatomic alignment when the hand moves through its motion arc about the wrist joint under physiological loads. In particular, scapholunate (SL) ligament injury could alter the carpal bones kinematics. Extensive studies have been conducted over the years but failed to quantify the inter-carpal bone kinematics due to its complex architecture. In this study, we focused on the scaphoid kinematics with respect to lunate based on 3 identified regions: proximal pole, waist and distal pole, after a simulated SL ligament injury during radioulnar deviation.

METHOD

Three cadaveric right hands were scanned using 64-slice dual source CT scanner (*Somatom Definition, Siemens Healthcare, Forchein, Germany*). The scans of hands were divided into 2 groups: (1) Intact SL ligament; (2) complete disruption of SL ligament. During the scan, each hand was passively moving from 20° ulnar deviation (UD) to 10° radial deviation (RD) [1,2] and images were taken at 3 different position: UD, RD and neutral.

After 3D reconstruction of the scaphoid and lunate using Mimics 19.0 (*Materialise NV, Leuven, Belgium*), the scaphoid was further sectioned into 3 regions: proximal pole, waist and distal pole (as shown in Figure 1a). The kinematics of the scaphoid were analyzed by using Matlab (*Mathworks, Natwick MA, USA*) based on the magnitude of displacement of the centroids at each region. The kinematics of the scapholunate joint was analyzed based on the displacements at the dorsal and volar points of the lunate and scaphoid's proximal pole, and the percentage of joint contact between the two bones. The joint contact was computed based on the distance of the vertex points within a threshold distance of 1 mm or less from the opposing joint surface.

RESULTS

The displacement at the scaphoid's proximal pole increased by 45% (from 1.89mm to 3.41mm) after complete disruption of the SL ligament, while the displacement at distal pole increased from 3.99mm to 4.58mm (Figure 1b). The displacement between scaphoid and lunate increased at both volar and dorsal points after division of the SL ligament, with the highest difference when the wrist was deviated radially (volar increased by 1.7mm; dorsal increased by 1.2mm). However, minimal changes were observed when the wrist was deviated ulnarly (displacement at volar was 0.56mm but subtle changes at the dorsal region). It was also observed that the percentage of joint contact between scaphoid-lunate occurred mostly at the dorsal region, with the highest contact at RD (25% contact between bones) and lowest at UD (9% contact) (Figure 1c).
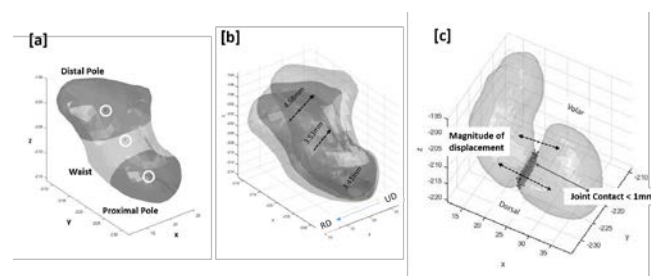

Figure 1: [a] Scaphoid kinematics was analysed based on 3 identified regions. [b] Magnitude of displacements from RD to UD. [c] Displacement and joint contact measurement between scapholunate joint.

CONCLUSIONS

The findings imply that the change of scaphoid kinematics could affect its surrounding bones, particularly at the distal radius without the SL ligament. We postulated that this may contribute to the progression of wrist osteoarthritis in the earlier stages, which usually occurred at the radial styloid-scaphoid junction and the radioscaphoid joint [3].

References

1. Mat Jais IS, Tay SC. Clin Radiol, 72(9):794, 2017

2. Mat Jais IS, Liu X, An KN, Tay SC, 36(12):1699-1703, 2014

3. Weiss KE, Rodner CM. J Hand Surg (Am), 32(5):725-46, 2007

Ita Suzana Mat Jais; ita.suzana.mat.jais@sgh.com.sg

EXPLORING LESSER KNOWN MECHANISMS OF STRUCTURAL FAILURE IN MECHANICALLY-INDUCED DISC HERNIATIONS

Vonne M. van Heeswijk[1], Peter A. Robertson[2], Ashvin Thambyah[1] and Neil D. Broom[1]
[1]**Experimental Tissue Mechanics Laboratory, Department of Chemical and Materials Engineering, University of Auckland, NZ.** [2]**Department of Orthopaedic Surgery, Auckland City Hospital, NZ.**

INTRODUCTION

Disc herniations have been reported to occur predominantly in the posterior and posterolateral regions of the disc [1]. Previous studies have investigated the structure-related failure processes of herniations induced mechanically *in vitro* in these two regions of healthy ovine lumbar motion segments [2]. However, little attention has been given to other regions of the disc annulus. A set of related topics were addressed: whether additional annular regions can be involved in a herniation event [3], whether a needle puncture as employed in provocative discography is able to influence where herniation might occur [4], and a proposed mechanism that could influence the vulnerability of the annulus to disruption.

METHOD

Healthy ovine lumbar motion segments with intact facet joints were divided into three groups: unpunctured controls (n = 14), punctured with 25Ga needle (n = 8), punctured with 18Ga needle (n = 8). All punctures were posterolateral as is commonly the case in provocative discography [5]. Each motion segment was compressed while flexed to induce failure [2]. The compression test was video-recorded to measure the induced downward and forward displacements of the superior vertebra. The internal structure of the disc was analyzed macroscopically by progressively sectioning it transversely to assess the total disc volume.

RESULTS

Of the 14 control discs 11 revealed disruption in the inner lateral annulus. For the needle-punctured discs no nuclear material passed through the 25Ga puncture whereas in 6 of the 8 discs with the 18Ga puncture it did. Further, for each of the two punctured groups 6 discs exhibited disruption of their inner lateral annuli, and for all three groups this lateral disruption was almost always associated with circumferential nuclear migration towards the posterolateral aspect of the disc (see Figure 1).

The mechanical testing induced anterior shear that was similar in magnitude to the downward displacement. Microstructural analysis of the lateral annulus of motion segments chemically fixed in their neutral posture (n = 5) or in anterior shear (n = 5) revealed that

Figure 1. Inner lateral annular disruption with circumferential migration of nuclear material towards the posterolateral region (see dashed arrow).

the fibre sets tilted counter to the direction of shear were always more relaxed while those tilted towards this direction were more often stretched. We argue that the vulnerability of the lateral annulus is increased by the component of anterior shear resulting in a grossly uneven load-recruitment between the oblique and counteroblique fibre sets.

CONCLUSIONS

The studies have identified a relatively unknown region, the lateral inner annulus, to be most vulnerable to disruption under the mechanical conditions employed, and can result in an eventual herniation in the well-known posterior or posterolateral aspects. Anterior shear recruits the annular fibres in the lateral annulus unevenly, making it more prone to early inner disruption. Interestingly, disruption resulting from the punctures did not lessen this vulnerability of the lateral annulus.

REFERENCES

1. Spine, 17, 1309–1315.

2. Spine, 39, 1018–1028.

3. Spine, 42, 1604-1613.

4. Spine, 43, 467-476.

5. Spine, 25, 1373-1381.

Speaker's name: Vonne van Heeswijk
Email address: vvan131@aucklanduni.ac.nz

EFFECTS OF LOWER LIMB ANTHROPOMETRY ON GAIT STABILITY

Arif Sugiharto, Sandro Mihradi, Tatacipta Dirgantara, Andi Isra Mahyuddin
Faculty of Mechanical and Aerospace Engineering, Institut Teknologi Bandung, Indonesia

INTRODUCTION

Human gait analysis has been widely employed in many areas, such as product design, medical rehabilitation, and sport. To study human gait parameters and characteristics, Biomechanics Research Group at Institut Teknologi Bandung have developed an affordable three-dimensional motion analyzer system. This system has been used to collect gait parameter of Indonesian (Chandra et al). Investigation of gait could be further extended to include stability and variability analysis. These analyses are widely used in gait identification (Yakhdani et al.).

Another consideration in the stability and variability analysis is the effect of anthropometry data. Indonesian people have varying anthropometry specifically on lower body extremities (thigh length, calf length, and foot length). The variance of ratio of lower limb length may affects the stability of gait. Therefore, the effects of lower limb anthropometry data on the gait stability is investigated in the present study.

METHOD

In this study, six normal subjects were instructed to walk on the treadmill at their normal comfortable speed and their motion is recorded by a 3D optical motion analyzer. Seven markers were attached on anatomical landmarks of their lower limb, i.e. pelvis, hip, mid-thigh, knee, mid-shank, ankle, and toe. The motion analyzer utilizes two 90 fps (frame per second) cameras to record the motion of the markers during gait. For each subject, data were taken for up to ten gait-cycles. Stability analysis is conducted by Maximum Lyapunov Exponent (λ_S), (Bruijn et al.) using Equation 1.

$$d(t) = D_0 e^{\lambda st} \qquad (1)$$

where D_0 and $d(t)$ are the initial divergence and divergence at specific time t, respectively. Variable λ is Lyapunov Exponent. The divergence is calculated from the distance of an observed point to its neighbor point but in the other gait cycle. The instability of kinematic gait parameter is evaluated based on the value of Lyapunov Exponent. In this study, the correlation between anthropometric data and gait stability was represented by coefficient of determination, R^2.

RESULTS

The effect of ratio between thigh length (*TL*) and calf length (*CL*) as well as calf length (*CL*) and foot length (*FL*) to the knee and ankle joint stability, respectively, were investigated. (Figure 1) presents the correlation value of *CL/FL* ratio to the instability of ankle joint in the frontal and sagittal planes. Similar to the effect of TL/CL, higher *CL/FL* also increases the instability of ankle joint, as indicated by the increase of λ_S value. Higher λ_S means the subjects would have more difficulty to maintain their stability. Higher R^2 on the frontal plane (medio-lateral direction) agrees with the finding of O'Connor et al.
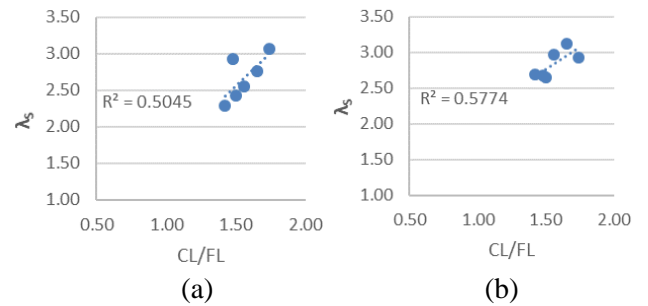

Figure 1. Correlation between *CL/FL* and Maximum Lyapunov Exponent (λ_S) of ankle joint on (a) sagittal plane (b) frontal plane.

CONCLUSIONS

Based on the preliminary experimental data, the correlation of gait stability of knee to the thigh to calf length ratio is significant on the frontal plane, not on the sagittal plane. While the correlation of gait stability of ankle to the calf to foot length ratio are observed on both frontal and sagittal planes.

Results in the present study imply that higher ratio of *TL/CL* and *CL/FL* will increase the instability of gait in the medio-lateral direction. Instability in the medio-lateral direction is associated with the risk of falling during subject walking. As a result, people with higher TL/CL or CL/FL ratios may have higher possibility of falling down.

REFERENCES

D. Chandra et al., Proc. Manufacturing, 2, 268-274, 2015.

H.R. F. Yakhdani et al., Clinical Biomech., 25, 230-236, 2010.

S.M. Bruijn et al., Med. Eng. & Physics, 34, 428–436, 2012.

O'Connor et al., J Neurophysiology, 102(3), 1411-9, 2009.

Sandro Mihradi (sandro@ftmd.itb.ac.id)

BONE MICROARCHITECTURE DAMAGE DUE TO PRESS-FIT FEMORAL KNEE IMPLANTATION QUANTIFIED USING HR-PQCT AND DIGITAL VOLUME CORRELATION

[1]Sophie Rapagna, [2]Sanaz Berahmani, [3]Caroline E Wyers, [3]Joop PW van den Bergh, [1]Karen J Reynolds, [4]Gianluca Tozzi, [2]Dennis Janssen and [1]Egon Perilli

[1]Medical Device Research Institute, College of Science and Engineering, Flinders University, Adelaide, SA
[2]Radboud University Medical Center, Orthopaedic Research Lab., Nijmegen, the Netherlands
[3]Dept. of Internal Medicine, VieCuri Medical Centre; Maastricht Univ., Venlo and Maastricht, the Netherlands
[4]Zeiss Global Centre, School of Engineering, University of Portsmouth, UK

INTRODUCTION

During prostheses press-fit implantation, high compressive and shear stresses at the implant-bone interface are generated. Permanent bone damage occurs [1], but the extent remains unknown.

The aim of this study is to quantify, using high-resolution peripheral quantitative computed tomography (HR-pQCT) and Digital Volume Correlation (DVC), permanent bone changes and deformation due to press-fit femoral knee implantation.

METHOD

Pre-implantation scan: Six human cadaveric distal femora (85±3 years) were resected and scanned with HR-pQCT (XtremeCT II, Scanco) at 60.7µm/voxel.

Implant fitting: An experienced surgeon fitted the femurs with a cementless cruciate retaining femoral knee implant Sigma® (DePuy Synthes, UK) with porous surface coating (Porocoat).

Post-implantation scan: Implants were then carefully removed and femurs rescanned with HR-pQCT.

Image Registration: 3D image-registration of pre- and post-implantation cross-section images was performed (DataViewer, Skyscan-Bruker).

Image Analysis: For each femur, volumes of interest (VOI) were selected (CT-Analyzer, Skyscan-Bruker) in the posterior-medial and posterior-lateral condyles and anterior flange; VOIs included 10 mm of depth in the coronal plane at the bone-implant surface. The bone volume fraction (BV/TV) for the VOIs in pre- and post-implantation images and their ratio (BV/TV$_{post}$ / BV/TV$_{pre}$) was calculated, slice by slice, at increasing depth.

Digital Volume Correlation: DVC direct correlation (DaVis, LaVision) [2] (3-step multipass, final subvolumes 20 voxels, 1.2 mm) was applied on the same VOIs pre- and post-implantation, to assess trabecular bone displacements and plastically accumulated strains.

RESULTS

The "BV/TV$_{post}$ / BV/TV$_{pre}$ ratio vs. depth" graphs (Fig. 1a) showed, consistently among the six femurs, three characteristic points, differing significantly in BV/TV$_{post}$ / BV/TV$_{pre}$ ratios and depth among them (p<0.05, Friedman and Wilcoxon signed rank tests), indicating: bone removal (A, ratio<100%), compaction (B, ratio>100%) and correspondence between pre- and post-implantation (C, ratio=100%) (Fig.1a, b).

On average, peak bone removal (A, BV/TV$_{post}$ / BV/TV$_{pre}$ ratio= 18±19%, mean±SD) occurred at 0.1±0.1mm depth, peak bone compaction (B, ratio= 135±28%) at 0.9±0.4mm, correspondence (C, ratio= 99±3%) at 2.1±0.5mm.

Correspondingly, the trabecular bone displacement computed by DVC for the 6 femurs suggested bone compaction up to 2.3±0.5mm depth (Fig.1c), with peak third principal strains of -150,500±39,500µε (mean absolute error 1,000-2,000µε, SD 200-500µε; Fig.1d), well above the yield strain of bone (7,000-10,000µε).
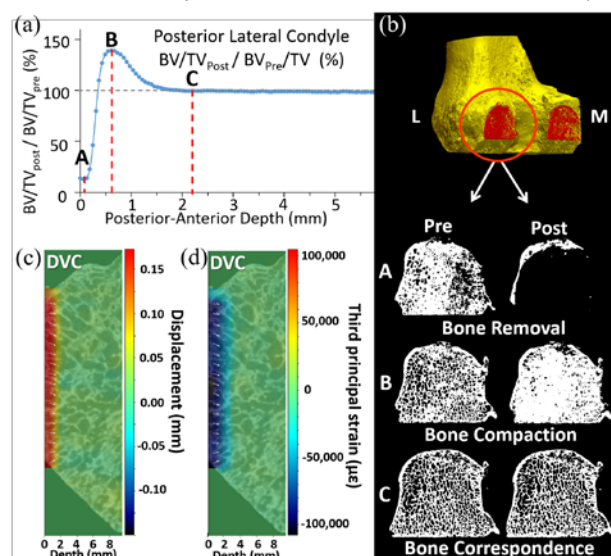

Figure 1. Femur posterior-lateral condyle, (a) "BV/TV$_{post}$ / BV/TV$_{pre}$ ratio vs. depth"; (b) HR-pQCT 3D posterior view (top), coronal cross-section images (bottom), pre- and post-implantation, at increasing depth; (c) DVC-computed displacements and (d) 3rd principal strains.

CONCLUSIONS

Combining high-resolution 3D-imaging and DVC enables to quantify permanent bone damage occurring after press-fit knee implantation. The apparent damage occurs up to 2 mm in depth, first with bone removal, followed by compaction and by no changes (correspondence). This data can be used to inform surgeons and manufacturers, advancing implant development.

REFERENCES

Bishop, N.E. J. Biomech. 47(6), 1472-1478, 2014
Tozzi, G. J. Mech. Behav. Biomed. Mater. 67, 117-126, 2011

SPEAKER INFORMATION

Egon Perilli, egon.perilli@flinders.edu.au

COMPARING CARTILAGE THICKNESS AND SUBCHONDRAL BONE MICROARCHITECTURE IN VARUS- AND VALGUS-ALIGNED OSTEOARTHRITIC TIBIAE WITH CONTROLS

[1]Sophie Rapagna, [1]Bryant Roberts, [2]Lucian B Solomon, [1]Karen J Reynolds, [2]Dominic Thewlis, [1]Egon Perilli

Medical Device Research Institute, College of Science & Engineering, Flinders University, Adelaide, SA
Centre for Orthopaedic & Trauma Research, The University of Adelaide, SA
Department of Orthopaedics and Trauma, Royal Adelaide Hospital, Adelaide, SA

INTRODUCTION

In knee osteoarthritis (OA), regional changes in proximal tibia subchondral trabecular bone (STB) microarchitecture and cartilage may reflect joint loading [1, 2]. However, reports on STB differences between OA and non-pathological joints are conflicting [3, 4]. Moreover, the effect of joint alignment on cartilage morphology (thickness) and underlying STB remains unexplored [1].

This analysis in an ongoing study aims to quantify tibia cartilage and STB microarchitecture in end-stage knee OA patients with varus or valgus-aligned joints, comparing them to control (non-OA) knees.

METHOD

Participants: Tibial plateaus were retrieved from 25 knee-OA patients (68±7 years, mass 90±18 kg; varus-aligned (n=18), valgus-aligned (n=7); knee arthroplasty) and from 15 cadavers (62±13 years, mass 83±16 kg; controls) free of musculoskeletal disease in the examined joint. OA joints were classified as varus- or valgus-aligned from the mechanical axis (pre-operative radiographs).

Micro-CT: The entire plateaus were micro-CT scanned (17 µm/voxel, model 1076, Skyscan-Bruker, Belgium). From the micro-CT images, cartilage thickness (Cg.Th) and the STB bone volume fraction (BV/TV) were analysed in four cylindrical subregions of interest (ROIs, 10mm diameter, 3-5mm length), in anteromedial (AM), anterolateral (AL), posteromedial (PM) and posterolateral (PL) condyles (Fig.1a,b). Medial-to-lateral (M:L) Cg.Th ratios and M:L BV/TV ratios among the 4 ROIs were also explored.

Statistics: Cg.Th, STB BV/TV and their M:L ratios for the varus-OA and valgus-OA group were compared to controls (Kruskal-Wallis test and Bonferroni-adjusted Mann-Whitney U-tests) Statistical significance, p<0.05.

RESULTS

Age and body mass did not significantly differ between OA and controls. Compared to controls, varus-OA exhibited significantly lower Cg.Th in AM ROI (-59%, p<0.05), but higher laterally (up to +63%); in valgus-OA it was higher medially (+56% in PM ROI, p<0.05). Whereas in controls the Cg.Th M:L ratios were close to unity (range: 0.8-1.1, Fig.1c), in varus-OA they were all below unity (0.2-0.6, p<0.05) and in valgus-OA they were similar to or higher than in controls (up to +40%).

Compared to controls, BV/TV in varus-OA was significantly higher (up to +49%) medially (AM, PM), whereas in valgus-OA it was higher laterally (up to +76%, AL, p<0.05). In varus-OA, all M:L BV/TV ratios ranged between 1.6-2.4, whereas in controls between 0.9-2.1 (Fig.1d). In valgus-OA, they were lower (up to -48%, AM:AL and PM:AL, p<0.05) than in controls and closer to unity (0.8-1.1).
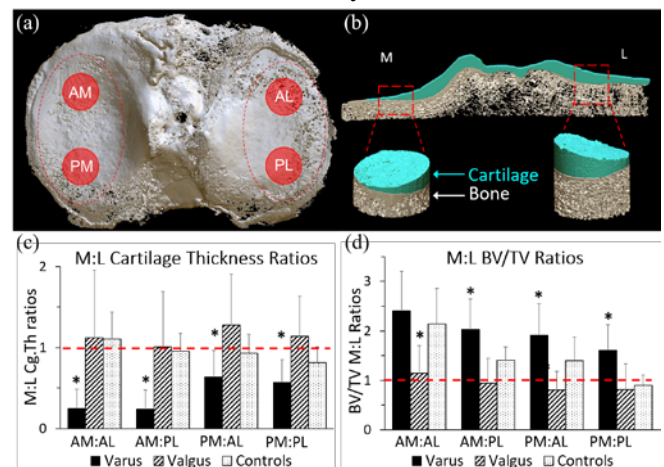

Figure 1. Top: micro-CT 3D rendering, (a) superior and (b) coronal view of a right tibial plateau, with the 4 ROIs examined; (c) average M:L Cg.Th ratios, (d) average M:L BV/TV ratios (error bars = standard deviation), dashed line indicates unity; *p<0.05 compared to controls.

CONCLUSIONS

OA and non-OA tibias differ significantly in Cg.Th and STB microarchitecture depending on joint alignment, suggesting that joint structural changes in OA may reflect differences in medial-to-lateral load distribution upon the tibial plateau. This may contribute to improve our understanding of the disease.

REFERENCES

Roberts, BC., J. Orthop. Res 35(9), 1927-1941, 2017.
Nakagawa, Y. Cartilage 6(4), 208-215, 2015.
Ding, M. J. Bone Joint Surg. Br. 85(6), 906-912, 2003.
Patel, V. J. Orthop. Res., 21(1), 6-13, 2003.

ACKNOWLEDGEMENTS

SPEAKER INFORMATION

Sophie Rapagna, sophie.rapagna@flinders.edu.au

ABC 11 - Program – DAY 1
Lecture theatre 505-011, Grafton Campus

3rd Dec 2018	
5.00 pm to 6.30 pm Session Chair: Dr Anna Murphy	**Special Session of the CLINICAL MOTION ANALYSIS GROUP (CMAG):** TRANSLATING TECHNOLOGY INTO THE CLINICAL GAIT LABORATORY • **Invited Speaker:** The use of patient specific neuromusculoskeletal modelling in clinical motion analysis - Dr Chris Carty • Gait model results are sensitive to impaired muscle size profiles in cerebral palsy – Geoffrey Hansfield (University of Auckland) • **Invited Speaker:** Assumptions in foot modelling: what are we ignoring - Dr Luke Kelly • Personalised 3d printing ankle-foot orthoses for children with charcot-marie-tooth disease – Elizabeth Wojciechowski (University of Sydney) PANEL DISCUSSION on: "How well are we translating technology into the clinical gait laboratory?"

GAIT MODEL RESULTS ARE SENSITIVE TO IMPAIRED MUSCLE SIZE PROFILES IN CEREBRAL PALSY

[1,2]Celine Marquette, [1,2]Alexandre Gerzaguet, [3,4]Ye Ma, [3]Yanxin Zhang, [1]Thor Besier, and [1]Geoffrey Handsfield

[1]Auckland Bioengineering Institute, University of Auckland; [2]Dept of Mechanical Engineering, SIGMA-Clermont, France; [3]Dept of Exercise Sciences, University of Auckland
[4]Faculty of Sports Science, Ningbo University, China

INTRODUCTION

Musculoskeletal models are valuable for estimating individual muscle force contributions to gait. While widespread use of musculoskeletal modelling for cerebral palsy (CP) is attractive, it is not commonplace, especially in a clinical setting. This is partly because muscle architecture—physiological cross sectional area, fibre length, and pennation angle—in musculoskeletal modelling packages is based on typically developing (TD) cadaver data whereas muscle architecture differs substantially in CP compared to TD [1]. The purpose of this study is to integrate CP-specific muscle architectures from prior MRI studies into musculoskeletal simulations of CP gait to investigate how sensitive are simulated muscle activations to different models of muscle architecture.

METHOD

We recorded marker data and ground reaction forces of 1 CP subject with crouch gait during overground barefoot walking for one gait cycle. We developed six muscle models based on CP-specific muscle architecture[1,2] and also used the generic model Gait2392 in OpenSim. The first two models were based on TD musculature and were the **TD generic model** (Gait2392) and the **TD scaled model** which was based on relationships reported in [2] and scaled to our subject's height and mass. The next two models—**CP average** and **CP crouch average**—were based on average muscle sizes reported in [1] for the entire CP population and for the three CP crouch subjects, respectively. The last three models—**CP crouch 1**, **2**, &**3**—were based on the specific muscle architectures reported for each of the three crouch subjects included in [1]. We simulated muscle activation in OpenSim for each model and compared the results across CP and TD muscle models.

RESULTS

On average, simulated activations for CP models were 33% greater than the TD generic model. The average crouch model differed by 34% averaged across all muscles, the average CP model was 20% different, and the TD scaled model differed by 18.5%. Maximum differences exceeded 100% for individual muscles. For certain muscle groups, e.g. the knee extensors, reduced muscle sizes in CP yielded increased activations (Figure 1). In other cases, such as the psoas, reduced muscle sizes promoted reduced activations, compensated by agonist muscles. This is reflective of the relative sizes of muscles, agonists, and the cost function of minimizing activations squared.
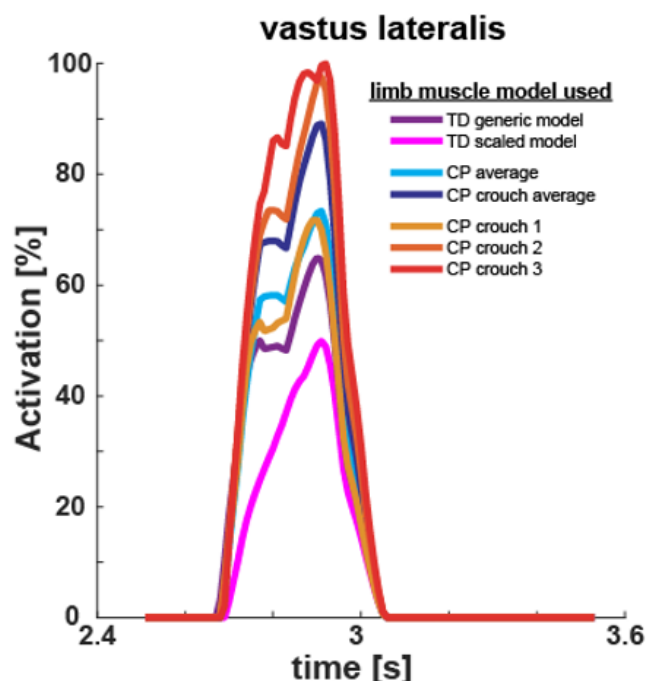

Figure 1. Different muscle models produce large variations in simulated activation. Vastus lateralis shown as representative muscle.

CONCLUSIONS

This study demonstrates the degree to which musculoskeletal simulation results differ between generic and physiologically reasonable CP muscle architectures. In the future, simulation results may be improved by direct imaging of a patient's muscle architecture and by EMG-driven simulations.

REFERENCES

1. Handsfield, et al. (2016). Muscle & nerve 53(6): 933-945.
2. Handsfield, et al. (2014). Journal of biomechanics, 47(3), 631-638.
Geoffrey Handsfield, g.handsfield@auckland.ac.nz

PERSONALISED 3D PRINTING ANKLE-FOOT ORTHOSES FOR CHILDREN WITH CHARCOT-MARIE-TOOTH DISEASE

Elizabeth Wojciechowski[1,2], David Little[1,2], Manoj P Menezes[1,2], Sean Hogan[2], Tegan L Cheng[1,2] and Joshua Burns[1,2]
[1]The University of Sydney, New South Wales, Australia
[2]Sydney Children's Hospitals Network, New South Wales, Australia

INTRODUCTION

Children and adolescents with Charcot-Marie-Tooth disease (CMT) are often prescribed ankle-foot orthoses (AFO) to manage lower limb impairments such as foot drop. They are usually handmade by a plaster cast of the patient's lower limb followed by thermoplastic vacuum forming. This traditional approach provides limited design options, is labour-intensive and can be associated with long outpatient wait times. 3D printing, also known as additive manufacturing, has the potential to transform the way AFOs are designed, manufactured and delivered.

The aim of this study is to evaluate personalised 3D printed AFOs vs. traditional handmade AFOs on walking ability for children with CMT.

METHOD

A 3D printing design and validation pipeline for personalised AFOs in CMT was proposed and evaluated (Figure 1). This includes:

1. Acquiring 3D surface images of the lower limb using a 3D surface scanner
2. Generating a computer aided design (CAD) models of AFOs from the 3D surface images of lower limb
3. 3D printing working AFO prototypes using 3D printable thermoplastics
4. Optimising the design of the AFO to reduce weight and improve biomechanical function
5. Validating 3D printed vs. traditional handmade AFOs on foot drop (maximum ankle dorsiflexion angle during the swing phase of gait) using three-dimensional gait analysis

RESULTS

Impressions of the lower limb were successfully captured using the Eva handheld 3D surface scanner (Artec 3D, Luxemborg). 3D surface images were then imported into Rhinoceros CAD software (Robert McNeel & Associates). Using the 3D surfaces images, CAD models replicating the design of three traditional AFO designs (posterior leaf spring, hinged, and solid) were generated.

AFO designs were then optimised reduce weight and improve function of the device by introducing design features such as holes.

Prototypes of the traditional and optimised AFOs were manufactured using a state of the art industrial grade fused deposition modelling 3D printer (Fortus 450mc, Stratasys, MN, USA) in Nylon 12. The print orientation was adjusted to maximize strength in areas (foot plate and ankle) under load during gait.
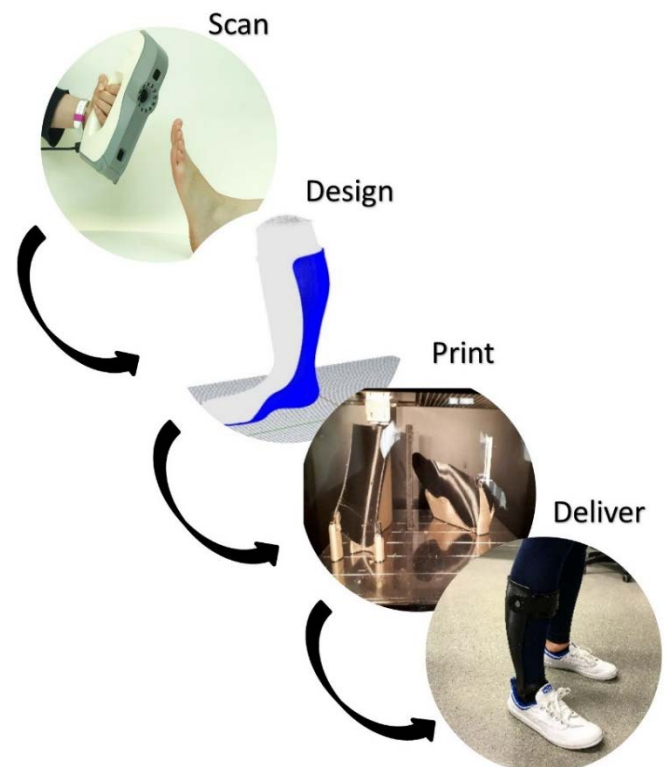

Figure 1. 3D printing AFO pipeline

CONCLUSIONS

The proposed 3D printing pipeline is a feasible work flow for the design, manufacture and delivery of AFOs. The use of 3D printing may offer many potential benefits over traditional manufacturing methods including improved biomechanical function, patient satisfaction and delivery time.

The effect of personalised 3D printed vs. traditional handmade AFOs on walking ability for children with CMT is currently being tested in a pilot crossover randomized controlled trial (printhotics™ trial) [1].

REFERENCES
 [1] ACTRN12618000558224p

Email: elizabeth.wojciechowski@sydney.edu.au